AD-A091 125 CALIFORNIA UNIV BERKELEY ELECTRONICS RESEARCH LAB F/G 20/5
EFFECTS OF THE CURRENT DISTRIBUTION ON THE CHARACTERISTICS OF T--ETC(U)
AUG 80 C Y CHEN, S WANG F49620-79-C-0178
UNCLASSIFIED AFOSR-TR-80-1030 NL

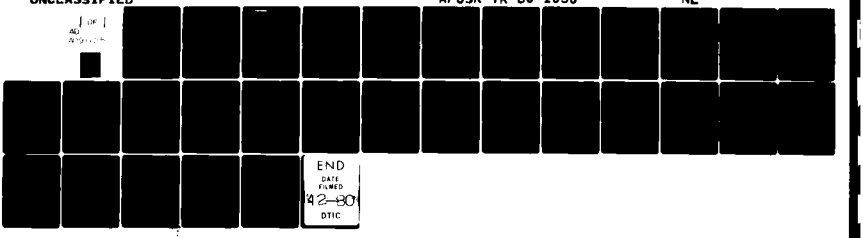

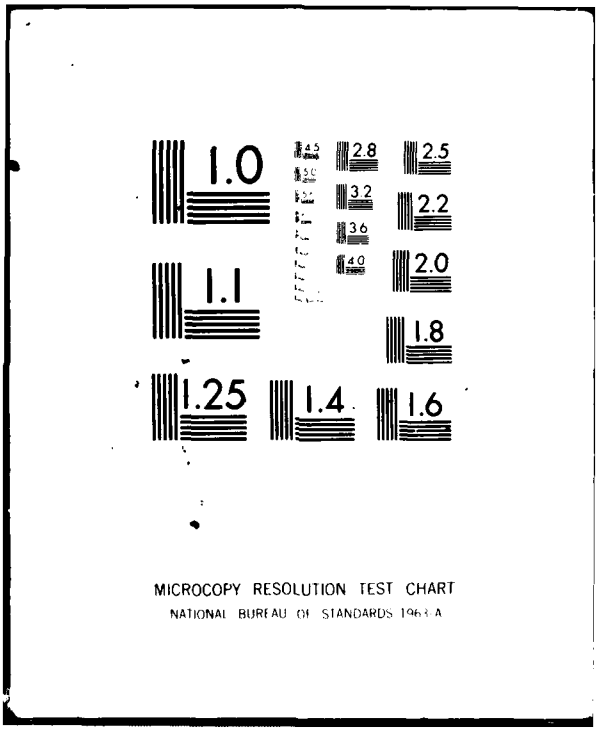
1.0
1.1
1.25
1.4
1.6
1.8
2.0
2.2
2.5
2.8
3.2
3.6
4.0
4.5
5.0
MICROCOPY RESOLUTION TEST CHART
NATIONAL BUREAU OF STANDARDS 1963-A

SECURITY CLASSIFICATION OF THIS PAGE (When Data Entered)

REPORT DOCUMENTATION PAGE

READ INSTRUCTIONS BEFORE COMPLETING FORM

1. REPORT NUMBER: AFOSR-TR-80-1030	2. GOVT ACCESSION NO: AD-A091125
3. RECIPIENT'S CATALOG NUMBER	
4. TITLE (and Subtitle): EFFECTS OF THE CURRENT DISTRIBUTION ON THE CHARACTERISTICS OF THE SEMICONDUCTOR LASER WITH A CHANNELED-SUBSTRATE PLANAR STRUCTURE	5. TYPE OF REPORT & PERIOD COVERED: Interim
6. PERFORMING ORG. REPORT NUMBER	
7. AUTHOR(s): Chung Yih Chen, Shyh Wang	8. CONTRACT OR GRANT NUMBER(s): F49620-79-C-0178
9. PERFORMING ORGANIZATION NAME AND ADDRESS: Dept. of Electrical Engineering & Computer Sciences, Univ. of California, Berkley, CA 94720	10. PROGRAM ELEMENT, PROJECT, TASK AREA & WORK UNIT NUMBERS: 2305/D9, 61102F
11. CONTROLLING OFFICE NAME AND ADDRESS: AFOSR, Bolling AFB, Washington, DC 20332	12. REPORT DATE: August 80
	13. NUMBER OF PAGES: 28
14. MONITORING AGENCY NAME & ADDRESS (if different from Controlling Office)	15. SECURITY CLASS. (of this report): Unclassified
	15a. DECLASSIFICATION/DOWNGRADING SCHEDULE

16. DISTRIBUTION STATEMENT (of this Report)

Approved for public release: Distribution unlimited

17. DISTRIBUTION STATEMENT (of the abstract entered in Block 20, if different from Report)

18. SUPPLEMENTARY NOTES

19. KEY WORDS (Continue on reverse side if necessary and identify by block number)

20. ABSTRACT (Continue on reverse side if necessary and identify by block number)

Effects of the current distribution along the junction plane on the lateral and longitudinal mode behaviors of the semiconductor laser with a channeled-substrate planar (CSP) structure are investigated experimentally and theoretically. A new laser structure of the double-current-confinement CSP type, which has two electrodes for pumping and only one channel for stimulated emission (TEPOSE), was employed for this study. Current distribution profile of this laser can be varied by changing the relative strength of the current in each electrode. Experimental results showed that an asymmetric current profile can degrade the fundamental-

DD FORM 1 JAN 73 1473 EDITION OF 1 NOV 65 IS OBSOLETE

UNCLASSIFIED

lateral mode operation. A theoretical model based on phase-locked two-mode excitation was developed to account for the far-field pattern of a TEPOSE laser with only one electrode excited. It is also found that nonuniform excitation over the lasing mode can lead to multi-longitudinal mode, probably due to nonuniformity in the quasi-Fermi level separation. The present study demonstrates the importance of symmetric and uniform current distribution in designing semiconductor lasers.

EFFECTS OF THE CURRENT DISTRIBUTION ON THE CHARACTERISTICS OF THE SEMICONDUCTOR LASER WITH A CHANNELED-SUBSTRATE PLANAR STRUCTURE

Chung Yih Chen and Shyh Wang

Department of Electrical Engineering and Computer Sciences
and the Electronics Research Laboratory
University of California, Berkeley, California 94720

ABSTRACT

Effects of the current distribution along the junction plane on the lateral and longitudinal mode behaviors of the semiconductor laser with a channeled-substrate planar (CSP) structure are investigated experimentally and theoretically. A new laser structure of the double-current-confinement CSP type, which has two electrodes for pumping and only one channel for stimulated emission (TEPOSE), was employed for this study. Current distribution profile of this laser can be varied by changing the relative strength of the current in each electrode. Experimental results showed that an asymmetric current profile can degrade the fundamental-lateral mode operation. A theoretical model based on phase-locked two-mode excitation was developed to account for the far-field pattern of a TEPOSE laser with only one electrode excited. It is also found that nonuniform excitation over the lasing mode can lead to multi-longitudinal mode, probably due to nonuniformity in the quasi-Fermi level separation. The present study demonstrates the importance of symmetric and uniform current distribution in designing semiconductor lasers.

I. INTRODUCTION

In the last few years, a considerable amount of effort has been directed toward the study of lateral mode stabilization in the semiconductor laser. It is generally believed that a built-in refractive index difference along the junction plane (lateral direction) of the laser structure is indispensable. Semiconductor lasers with linear light-current (L-I) relation, stable fundamental lateral mode, and single longitudinal mode, such as BH [1,2], CSP [3,4], and TJS [5] lasers, have been widely reported.

Since lasing action in a semiconductor laser is provided by the radiative recombination of electrons and holes, one can see that the current distribution in the laser structure should affect the lateral mode and/or the longitudinal mode behavior either directly or indirectly. Study in this area not only promotes one's understanding of the semiconductor laser, but also provides useful information on the laser design. Some workers have reported the effect of asymmetric gain profile on the far-field radiation pattern [6,7]. However, the work was limited to the case of the oxide stripe laser, which has no built-in index profile for lateral mode stabilization. Consider a laser structure with a built-in refractive index profile along the junction plane as shown in Fig. 1(a), and an asymmetric current distribution shown in Fig. 1(b). This asymmetric current profile can be introduced either by the fabrication process or by the lasing action itself. One important effect of this asymmetric current profile on the lateral mode stabilization can be argued as follows. The refractive index profile shown in Fig. 1(a) defines a set of normal modes in the lateral direction. Whether a mode can lase or not depends on whether or not its modal gain reaches the lasing threshold. Since the modal gain depends on the overlap integral of the

modal intensity and the spatial gain profile, it is expected that the first order mode may acquire a modal gain comparable to or even higher than that of the fundamental mode in view of their field distribution shown in Fig. 1(c). Under such conditions, the lateral-mode behavior becomes complicated and unstable with respect to the pumping levels because the relative phase and the power sharing between the modes are beyond one's control.

In this paper, we present the experimental and theoretical study on the effects of the current distribution on the modal stability in a laser structure with a built-in refractive index difference along the junction plane. Some preliminary results on this topic were presented recently [8]. We have fabricated a laser structure of the double-current confinement channeled-substrate planar type [4] for this study. This laser structure is unique in that it has two electrodes for pumping and one channel for stimulated emission (TEPOSE for short). Current distribution with respect to the built-in channel can be varied at one's disposal by changing the ratio of the current flowing through the two electrodes. It is shown that asymmetric current distribution is detrimental to the stable fundamental lateral-mode operation. Moreover, we observed that asymmetric current profile usually led to multi-longitudinal mode operation. A theoretical model based on the phase-locked two-mode excitation is then presented to explain the far-field pattern of a laser with asymmetric current distribution. The calculated results are in agreement with the experiment. Finally, a possible reason for the multi-longitudinal mode operation and means to provide a symmetric and uniform current distribution are discussed.

II. EXPERIMENT

A. Device Fabrication

A schematic cross-section and an SEM photograph of the TEPOSE laser used for the present study are shown in Fig. 2(a) and (b), respectively. The fabrication procedures of the device consist of a two-step LPE growth. A layer of p^+-GaAs was first grown. Conventional photolithographic process was applied to groove a set of 4.5 μm channels on the wafer. This was then followed by the second LPE to grow n-$Ga_{0.65}Al_{0.35}As$, p-$Ga_{0.88}Al_{0.12}As$, p-$Ga_{0.65}Al_{0.35}As$, p-GaAs, and n-GaAs. After the second LPE, the original photomask was employed again to open two contact stripes using double exposure. Care should be exercised to assure that chemical etching penetrated through the n-GaAs layer. The separation between the edge of the contact opening and the center of the bottom channel is 4.3 μm (L_1) and 3.4 μm (L_2), respectively. Gold was applied over the whole wafer for the p-type contact. Once again, the original photomask was used to provide opening for electrode isolation by Au etching. Particular attention was paid to prevent gold film from peeling off because of the lateral etching. Since a double current confinement scheme was used in the present structure, one can assure that current flows through the bottom channel instead of flowing directly downward from the contact opening. Notice that the minimum separation between the two electrodes was limited by the channel width of the photomask and the gold etching process. After Ge-Au was evaporated for the n-type contact, the wafer was cleaved into dice and mounted on TO-5 header. Gold wire was finally bonded to each electrode and the lasers were tested under pulsed excitation (800 ns duration, 58 Hz).

B. Measurement Technique

Current-voltage (I-V) characteristic of each device was first measured to assure that the device functioned properly in view of the

electrical property. Electrical isolation between the two electrodes was also examined by measuring the I-V characteristic. Resistance between the two electrodes ranged from 20 Ω to 30 Ω. This degree of isolation is considered to be sufficient in the sense that current distribution can be varied properly by changing the pumping current to each electrode, as will be shown later.

Current distribution along the junction plane was determined by measuring the spontaneous-emission profile below lasing threshold. This linear gain-current assumption is based on theoretical and experimental results [9,10]. An experimental setup for this measurement is shown in Fig. 3. Details of measurement had been presented elsewhere [11]. The intensity profile was obtained by imaging the near-field pattern of the laser onto a Si target of a RCA vidicon camera Model TC 1005 using a 40 x microscope objective with NA = 0.65. Raleigh resolution given by $\lambda/2NA$ is 0.6 μm, where λ is the vacuum wavelength. Video signal was first applied to the TV monitor and then to the oscilloscope for display. All the electronic units share the same trigger which is provided by the vertical drive of the vidicon camera. Care was given to synchronize the two pulses applied to the two electrodes.

C. Experimental Results

Current distribution along the junction plane monitored by spontaneous emission is shown in Fig. 4. Figure 4(a) and (b), respectively, correspond to the cases when electrode No. 1 and 2 are exclusively excited. Note that the center line of the oscillogram corresponds approximately to the center of the bottom channel. Exactly as one expected, the current distribution is indeed asymmetric with the peak occurring somewhere between the electrode and the center of the bottom channel. It is also interesting to note that the profile tailed off more slowly on

one side than the other. We believe that this was due to the current crowding effect introduced by the n-p reverse-biased junction on both shoulders of the channel region. If, however, both electrodes were pumped simultaneously, we successfully obtained a symmetric current profile with equal tailing on both sides by adjusting the current flowing through the two electrodes. It should be pointed out that arranging $I_1 = I_2$ can not guarantee a symmetric current profile. This is so because the spacing between the electrode and the center of the channel was not equal; and, therefore, the peak and the distribution in current did not occur symmetrically. For the particular diode under study, symmetric current profile corresponded to $I_1/I_2 = 1.2$. This asymmetry was also reflected in the current threshold with $I_{th1} = 150$ mA and $I_{th2} = 120$ mA.

Fig. 5(a) showed the near-field pattern of the laser with electrode No. 1 excited exclusively at $I_1 = 1.3\ I_{th1}$. This electrode was chosen simply to accentuate the degree of asymmetry. On the other hand, if both electrodes were excited simultaneously with $I_1/I_2 = 1.2$, a near-field pattern as shown in Fig. 5(b) was observed. Double traces in the pattern were due to a slight instability in the scope trace. The effect of asymmetric current distribution was readily observed from this comparison. Notice that a cladding layer thickness of 0.43 μm and Aℓ content of 0.12 in the active layer (referred to in Fig. 2) should give a built-in refractive-index difference greater than 8×10^{-3} based on the effective refractive index calculation by Aiki et al. [12]. This result then points to an important conclusion that a symmetric current distribution is indispendable for a stable fundamental-lateral-mode excitation even though a certain amount of built-in refractive-index difference was incorporated into the laser structure.

The comparison was also discernable based on the far-field pattern.

Fig. 6(a) shows the far-field pattern corresponding to the case with electrode No. 1 being excited only. The patterns were composed of two lobes with the relative intensity roughly independent of pumping levels. This far-field radiation pattern is not to be confused with the non-Gaussian far-field pattern observed in narrow ($\leq$ 6 μm) stripe-geometry lasers reported by many workers [7,13-15]. Semiconductor lasers with CSP structure [3,4] typically show stable Gaussian-like far-field patterns even if the channel width is as small as 2 μm. Now, if both electrodes were pumped to give a more symmetric current distribution, the far-field patterns shown in Fig. 6(b) were observed. These patterns were more stable and controllable, although a tiny side lobe did come into existence.

We also extended our efforts to study the effect of current distribution on the longitudinal-mode behavior. Up to the present time, single longitudinal-mode operation of the semiconductor laser was not reproducible although it had been reported by many researchers [4,12,16,17]. The reason for causing multi-longitudinal mode operation has not been conclusively identified, although several hypotheses were advanced [17-19]. Our experimental results showed that multi-longitudinal mode was invariably observed if only one electrode was excited in the TEPOSE laser. Fig. 7 shows the typical spectra at various pumping levels of the TEPOSE laser with only one electrode being excited. Not only were multi-longitudinal modes observed at each current level, but also the envelope of the spectrum moved toward longer wavelength. A possible reason for these observations will be given later.

III. THEORETICAL MODEL

A. Model of Phase-locked Two-Mode Excitation

First, we looked for the normal modes that can be supported by the

built-in waveguide. Considering the laser structure shown in Fig. 2, we may well assume the built-in refractive index profile to have the forms shown in Fig. 8, where n(x) is the real part of the complex refractive index $\bar{n}(x)$, and $\alpha(x)$ is the absorption coefficient. The abscissa is along the lateral direction with the origin located at the center of the bottom channel. Now, one can expand the index n(x) into a Taylor series

$$n(x) = \sum_{m=0}^{\infty} A_{2m} x^{2m} \tag{1}$$

for $|x| < \frac{S}{2}$, where S is the channel width. Only even-power terms were retained since the bottom channel is symmetric with respect to its center. To a first-order approximation, one can truncate all the terms higher than second order and reach the form

$$n(x) \approx A_0 + A_2 x^2 \tag{2}$$

This profile can also be expressed in terms of the parameters of the structure as follows:

$$n(x) \approx n_0 - (4 \Delta n_p/S^2) x^2 \tag{3}$$

where n_0 is the peak index at x = 0, and $\Delta n_p = n_0 - n(S/2)$ is the largest variation in n(x).

Similar manipulation can also be applied to $\alpha(x)$, which is then given by

$$\alpha(x) \approx \alpha_0 + (4 \Delta\alpha/S^2) x^2 \tag{4}$$

where $\alpha_0 = \alpha(0)$ and $\Delta\alpha$ is the largest variation in $\alpha(x)$. It should be pointed out that both n(x) and $\alpha(x)$ were introduced by the penetration of the radiation into the lossy substrate and by a built-in channel

region. Since $n(x)$ and $\alpha(x)$ are related to $\bar{n}(x)$ by

$$\bar{n}(x) = n(x) - i \frac{\alpha(x)}{2k_0} \tag{5}$$

and $\bar{\varepsilon}(x) = \bar{n}^2(x)$, $\bar{\varepsilon}(x)$ can be represented by

$$\bar{\varepsilon}(x) = \bar{\varepsilon}(0) - a^2 x^2 \tag{6}$$

where fourth-order term has been neglected because of increasing insignificance and $k_0 = 2\pi/\lambda$, λ is the vacuum wavelength, $\bar{\varepsilon}(x)$ is the complex dielectric constant, a is a complex number and can be expressed as $a = a_r + i\, a_i$ with a_r being the real part and a_i the imaginary part. The parameters $\bar{\varepsilon}(0)$, a_r, and a_i are given by

$$\bar{\varepsilon}(0) \approx n_0^2 \tag{7}$$

$$a_r \approx \left\{ \frac{4n_0 \Delta n_p}{S^2} \left(1 + \left[1 + \left(\frac{\lambda \Delta \alpha_p}{4\pi \Delta n_p} \right)^2 \right]^{1/2} \right) \right\}^{1/2} \tag{8}$$

$$a_i \approx \frac{n_0 \lambda \Delta \alpha_p}{\pi S^2 a_r} \tag{9}$$

where $n_0 >> \frac{\alpha_0}{k_0}$ has been used.

The two-dimensional wave equation to be solved is given by

$$\nabla^2 E_x + k_0^2\, \bar{\varepsilon}(x,y)\, E_x = 0 \tag{10}$$

with $\bar{\varepsilon}(x,y)$ given by

$$\bar{\varepsilon}(x,y) = \begin{cases} \bar{\varepsilon}(0) - a^2 x^2 & 0 \leq y \leq d \\ \varepsilon_1 & \text{elsewhere} \end{cases} \tag{11}$$

where ε_1 is the dielectric constant of the cladding layer. This equation has been considered by Paoli [20] and the approximate modal distribution along the junction plane is the well-known Hermite-Gaussian function given by

$$E_x^m(x) = C_m H_m[(a\, k_0\, \Gamma^{1/2})^{1/2}\, x] \exp\left(-\frac{\Gamma^{1/2}}{2}\, k_0\, a\, x^2\right) \qquad (12)$$

where E_x^m is the approximate modal field of mth order, H_m is the Hermite polynomial of order m, and Γ is the confinement factor in the vertical direction. The solution is by no means complete without knowing Δn_p and $\Delta\alpha_p$. These can be obtained using effective-refractive-index calculation [12] by assuming the channel to be infinitely deep.

If the field expressed in Eq. (12) is normalized so that $\int_{-\infty}^{\infty} |E_x^m|^2\, dx = 1$, then the coefficient C_m's are found to be [21]

$$C_m = 2^{-\frac{m}{2}}\, (m!)^{-\frac{1}{2}} \left(\frac{k_0\, a\, \Gamma^{\frac{1}{2}}}{\pi}\right)^{\frac{1}{4}} \qquad (13)$$

Since E_x^m is the eigenfunction of the boundary value problem defined by Eqs. (10) and (11), $\{E_x^m\}$ forms a complete set. Consequently, we can expand the lasing field of the TEPOSE laser with only one electrode excited into a generalized Fourier series

$$E_x(x) = \sum_{m=0}^{\infty} D_m\, C_m\, H_m\, [(k_o\, a\, \Gamma^{1/2})^{1/2}\, x]\, \exp\left(-\tfrac{1}{2}\, k_0\, a_r\, \Gamma^{1/2}\, x^2\right) \qquad (14)$$

where D_m's are the Fourier coefficient. Note that we have lumped the insignificant phase factor into D_m.

As a model for the analysis, we assume $D_m = 0$ for $m \geq 2$. In other words, only fundamental and first-order modes can be excited. We name this model as phase-locked two-mode excitation. The adoption of the phase-locked model arises from the observation that the far-field pattern shows two instead of three lobes. The fundamental and first-order fields can simply be written as follows:

$$\text{fundamental:} \quad A \exp\left(-\frac{1}{2} k_0 a_r \Gamma^{1/2} x^2\right) \exp(i\theta_0)$$

$$\text{first order:} \quad B\, x \exp\left(-\frac{1}{2} k_0 a_r \Gamma^{1/2} x^2\right) \exp(i\theta_1) \tag{15}$$

where A and B are two parameters, θ_0 and θ_1 are the phase of the fundamental and first-order modes, respectively.

Define two parameters C^* and θ^*

$$C^* \equiv \left|\frac{B}{A}\left(\frac{2}{k_0 a \Gamma^{1/2}}\right)^{1/2}\right| \tag{16}$$

$$\theta^* \equiv \theta_1 - \theta_0 \tag{17}$$

where C^* is a measure of the relative intensity between the first-order and the fundamental modes, with an increase in C^* corresponding to an increasing dominance of the first-order mode. The angle θ^* represents the phase difference between the first-order and the fundamental modes.

The far-field intensity I as a function of angle θ can be obtained by applying Kirchhoff-Huygens principle [22], and is given by

$$I(\theta) = D \cos^2\theta \left(1 - \frac{2C^* \sin\theta^* \sin\theta}{a_r} + \frac{C^{*2} \sin^2\theta}{a_r^2}\right) \exp\left(\frac{-k_0 \sin^2\theta}{a_r \Gamma^{1/2}}\right) \tag{18}$$

where D is a constant. Calculated results and comparison with the experiment will be shown in the following section.

B. Calculated Results

In the following calculation, the values $a_r = 0.1\ \mu m^{-1}$, $\lambda = 0.8\ \mu m$, and $\Gamma = 0.4$ were used. It is obvious that the only factor causing asymmetry in $I(\theta)$ is the second term in the first bracket of Eq. (18). If $\theta^* = 0$, which means fundamental and first-order modes have the same phase, $I(\theta)$ is always an even function of θ. For easy discussion, we consider the following cases, depending on the value of θ^* and C^*. Notice that

$a \approx a_r$ has been used in the calculation since $a_i << a_r$.

First, consider $\theta^* = 0$ and $C^* = 0.05$. As we pointed out previously, $\theta^* = 0$ always gives a symmetric far-field pattern. The value of C^* is considered to be so small that the far-field profile is dominated by the fundamental mode (referred to in Eq. 16). The calculated result is shown in Fig. 9(a).

As the value of C^* is increased, the far-field pattern is then dominated by the first-order mode. A calculated result for $\theta^* = 0$ and $C^* = 1.6$ is shown in Fig. 9(b).

Next, consider the case with $\theta^* = 90°$, which means the phase of the first-order mode leading that of the fundamental mode by 90°. The far-field pattern is no longer symmetric under this condition. A dominant lobe and a side lobe are usually obtained. The calculated result for $\theta^* = 90°$ and $C^* = 0.5$ is shown in Fig. 10(a). As the value of C^* is increased, the side lobe will grow. This is shown as a solid curve in Fig. 10(b) for the case of $\theta^* = 90°$ and $C^* = 2.5$. The experimental result is also duplicated and shown as a dashed curve in Fig. 10(b). Agreement between calculated and experimental results is reasonable. Although better agreement could be achieved by adjusting θ^* and C^*, no attempt was made to do that.

IV. DISCUSSION

Although the experiment was performed specifically on the CSP-type laser, some general observations can be made. If ideally the lateral index difference Δn and the channel width S are such that only the fundamental lateral mode can be supported, the effect of the current distribution on the laser performance would not be detrimental to mode stability. In practice, however, Δn and S are such that the dielectric waveguide may support two or even three modes in the lateral direction. In

this case, a symmetric and uniform current distribution plays an essential role in the laser performance. The result can also be applied to other laser structures such as BH and TJS.

As for the multi-longitudinal mode operation of the semiconductor laser, we present the following possible qualitative explanation. Consider two points A and B in the current profile shown in Fig. 1(b). Since point A has a higher current density, quasi-Fermi level separation there should be larger than that at point B. It is known that the spectral gain profile $g(\lambda)$ was calculated under the assumption of uniform quasi-Fermi level separation [23]. If the quasi-Fermi level separation is increased, $g(\lambda)$ will become broader with its peak value increased and shifted to higher energy [9]. Therefore, the effective spectral gain profile $g_{eff}^{m}(\lambda)$ which a particular lateral mode experiences is

$$g_{eff}^{m}(\lambda) = \frac{\int_{-\infty}^{\infty} g(x,\lambda) E_m^2(x)dx}{\int_{-\infty}^{\infty} E_m^2(x)dx} \tag{19}$$

It is known that averaging always causes broadening. Consequently, nonuniform excitation experienced by the lasing mode can lead to spectral broadening and thus to multi-longitudinal-mode operation. If only one electrode of the TEPOSE laser was excited, the current distribution would be nonuniform in the channel region. Based on the above argument, a multi-longitudinal mode operation can be expected, and was indeed observed in the experiment.

Although single longitudinal mode operation was not observed when both electrodes were excited, the whole spectral behavior was generally improved in the sense that the number of longitudinal mode was decreased. We attribute the lack of single longitudinal mode operation in the TEPOSE laser when both electrodes were excited to a strong dependence of the photon energy of the spectral gain peak on the pumping current. Based

on Stern's calculation [9], we estmated the rate of peak wavelength change $d\lambda/dJ$ to be 0.155 $\mathring{A}$ cm^2/A. Because of a considerably large spacing between the electrodes, (8 μm versus 4 μm channel width), we can expect a small dip at the center of the current profile when both electrodes are excited. Assuming that the small dip caused a 1% perturbation in the current distribution, we obtained a variation in the wavelength of the peak gain by 16 $\mathring{A}$. Therefore, the resultant spectral broadening is expected to be larger than the longitudinal mode spacing of 2.7 $\mathring{A}$ and can lead to a lack of single longitudinal mode operation. We should point out that the slight perturbation (assumed 1%) is beyond the detection of the present setup. Also this dip should not significantly affect the lateral mode because the difference between $g^m_{eff}(\lambda)$ with different m is large. However, the difference between $g^m_{eff}(\lambda)$ with the same m but different longitudinal modes is small. Therefore, a broadening comparable to the longitudinal mode spacing will be large enough to have an effect on the longitudinal mode behavior.

Since asymmetric current distribution in the lateral direction will be detrimental to the stable fundamental-mode operation, special care should be given to the photomask alignment of the contact opening with respect to the channel. One practical way of overcoming this problem is to provide a wider contact opening [4], which makes a slight misalignment tolerable. The current distribution experienced by the lasing mode will be more or less uniform in this case and hence favorable for single longitudinal-mode operation.

V. CONCLUSION

The effects of current distribution on the lasing characteristics of a semiconductor laser with CSP structure have been investigated experimentally and theoretically. A laser structure capable of supporting

a wide variety of current distribution profiles was fabricated for this study. Experimental results showed that asymmetric current distribution is detrimental to a stable fundamental-lateral-mode operation. This points to an important conclusion that symmetric current distribution is required for a stable lateral-mode operation even though a built-in index difference was incorporated into the laser structure. A theoretical model based on phase-locked two-mode excitation was presented to explain the far-field pattern of the TEPOSE laser with only one electrode excited. The agreement with the experimental results was good.

Semiconductor lasers with nonuniform excitation usually lead to multi-longitudinal mode operation. This is in contrast to single longitudinal-mode behavior observed in semiconductor lasers with uniform excitation. Multi-longitudinal mode may be caused by spectral broadening introduced by nonuniform quasi-Fermi level separation in the lateral direction.

A wider contact than the channel was generally considered favorable for fundamental lateral mode and single longitudinal mode operation of the CSP laser. In our view, the principal benefit of a wider contact was not the elimination of gain/loss guiding becuase $\Delta\alpha$ always exists, but rather the attainment of a uniform and symmetric current distribution for the fundamental lateral mode. In laser structures capable of supporting more than one lateral mode, a uniform and symmetric current distribution is as important as a built-in index for mode stability and single mode operation. This consideration should lead to an increase in reproducibility of the performance of semiconductor lasers.

Research supported by Air Force Office of Scientific Research Contract F49620-79-C-0178 and Army Research Office Grant DAAG29-77-G-0053.

References

[1] T. Trukada, J. Appl. Phys. 45, 4899 (1974).

[2] W. T. Tsang, R. A. Logan and M. Ilegems, Appl. Phys. Lett. 32 311 (1978)

[3] K. Aiki, M. Nakamura, T, Kuroda and J. Umeda, Appl. Phys. Lett. 30, 649 (1977).

[4] C. Y. Chen and S. Wang, Appl. Phys. Lett., 36, 634 (1980).

[5] H. Namizaki, H. Kan, M. Ishii and A. Ito, J. Appl. Phys. 45, 2785, (1974).

[6] J. Butler and H. S. Sommers, Jr., IEEE J. Quantum Electron. QE-14, 413 (1978).

[7] W. Streifer, R. D. Burnham and D. R. Scifres, IEEE J. Quantum Electron. QE-15, 136 (1979).

[8] C. Y. Chen and S. Wang, Topical Meeting on Integrated and Guided Wave Optics, Nevada, 1980 (unpublished).

[9] F. Stern, J. Appl. Phys. 47, 5382 (1976).

[10] B. W. Hakki and T. L. Paoli, J. Appl. Phys. 46, 1299 (1975).

[11] C. Y. Chen and S. Wang (to be published in Appl. Phys. Lett., Aug. 1, 1980, Ms. #9655L).

[12] K. Aiki, M. Nakamura, T. Kuroda, J. Umeda, R. Ito, N. Chinone and M. Maeda, IEEE J. Quantum Electron. QE-14, 89 (1978).

[13] T. Kobayashi, H. Kawaguchi and Y. Furukawa, Jpn. J. Appl. Phys. 16, 601 (1977).

[14] P. M. Asbeck, D. A. Cammack and J. J. Daniele, Appl. Phys. Lett. 33, 504 (1978).

[15] P. M. Asbeck, D. A. Cammack, J. J. Daniele and V. Klebanoff, IEEE J. Quantum Electron. QE-15, 727 (1979).

[16] W. Susaki, T. Tanaka, H. Kan and M. Ishii, IEEE J. Quantum Electron. QE-13, 587 (1977).

[17] D. R. Scifres, R. D. Burnham and W. Streifer, Appl. Phys. Lett. 31, 112 (1977).

[18] H. Statz, C. L. Tang and J. M. Lavine, J. Appl. Phys. 35, 2581 (1964).

[19] M. Yamada and Y. Suematsu, IEEE J. Quantum Electron. QE-15, 743 (1979).

[20] T. L. Paoli, IEEE J. Quantum Electron. QE-13, 662 (1977).

[21] E. Merzbacher, Quantum Mechanics, pp. 60, John Wiley, New York (1970).

[22] J. W. Goodman, Introduction to Fourier Optics, McGraw-Hill, 1968.

[23] G. Lasher and F. Stern, Phys. Rev. 133, A553 (1964).

Figure Captions

Figure 1. Illustration of a built-in index difference (a), asymmetric current distribution (b), and field distribution of fundamental mode $E_0(x)$ and first-order mode $E_1(x)$ along the junction plane (c). A and B represent two points of different excitation level.

Figure 2. Schematic diagram (a) and SEM micrograph (b) of a TEPOSE laser.

Figure 3. Schematic diagram of the experimental setup for current distribution and near-field measurement.

Figure 4. Current distribution in a TEPOSE laser with only electrode No. 1 excited (a), only electrode No. 2 excited (b), and both electrodes excited with $I_1/I_2 = 1.2$ (c). Horizontal white bar in (b) indicates the position of the bottom channel.

Figure 5. Near-field pattern of a TEPOSE laser (same as in Fig. 4) with electrode No. 1 excited ($I_1 = 1.3\ I_{th1}$) (a), and both electrodes excited ($I_1/I_2 = 1.2$) (b).

Figure 6. Far-field pattern of a TEPOSE laser (same as Fig. 4) with (a) only electrode No. 1 excited ($I_1 = 1.3\ I_{th1}$) and (b) both electrodes excited ($I_1/I_2 = 1.2$).

Figure 7. Spectra of a TEPOSE laser (same as in Fig. 4) with only electode No. 1 excited.

Figure 8. Illustration of the index profile (a) and absorption coefficient (b) introduced by the built-in channel in a CSP structure.

Figure 9. Calculated normalized far-field pattern of the TEPOSE laser with (a) $\theta^* = 0°$, $C^* = 0.05$ (dashed line) and (b) $\theta^* = 0°$, $C = 1.6$ (solid line).

Figure 10. Calculated normalized far-field pattern (solid line) of the TEPOSE laser, (a) $\theta^* = 90°$, $C^* = 0.5$, (b) $\theta^* = 90°$, $C^* = 2.5$. Dashed line in (b) shows the experimental result.

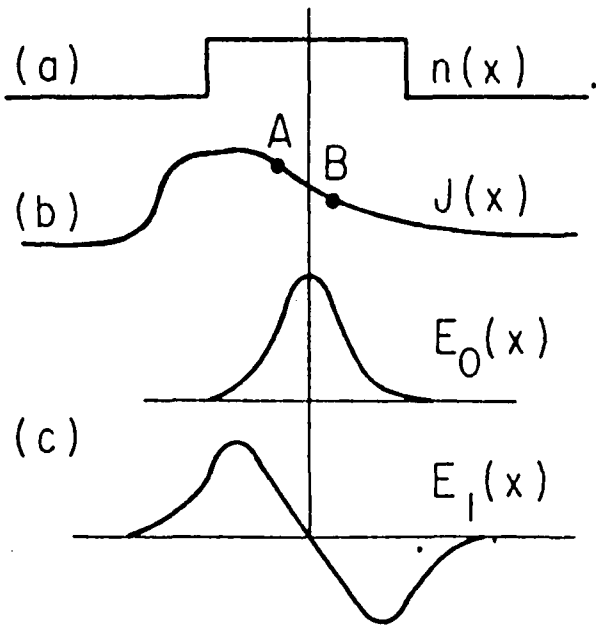
(a)
n(x)
A
B
(b)
J(x)
$E_0(x)$
(c)
$E_1(x)$

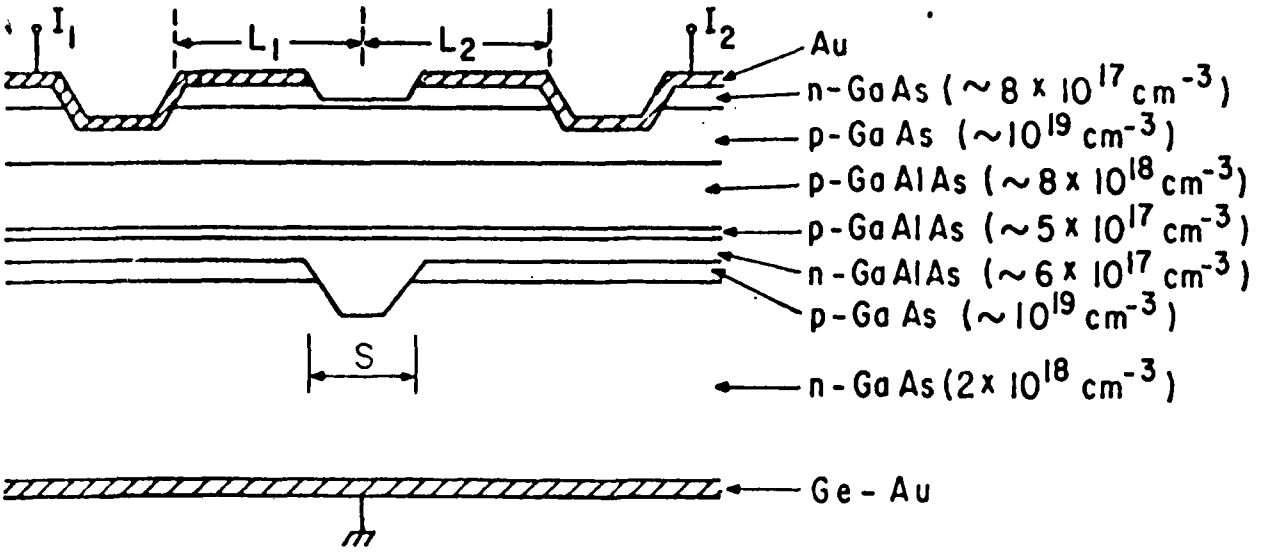
I1
L1
L2
I2
Au
n-GaAs (~8 x 10^17 cm^-3)
p-GaAs (~10^19 cm^-3)
p-GaAlAs (~8 x 10^18 cm^-3)
p-GaAlAs (~5 x 10^17 cm^-3)
n-GaAlAs (~6 x 10^17 cm^-3)
p-GaAs (~10^19 cm^-3)
S
n-GaAs (2 x 10^18 cm^-3)
Ge-Au

(a)

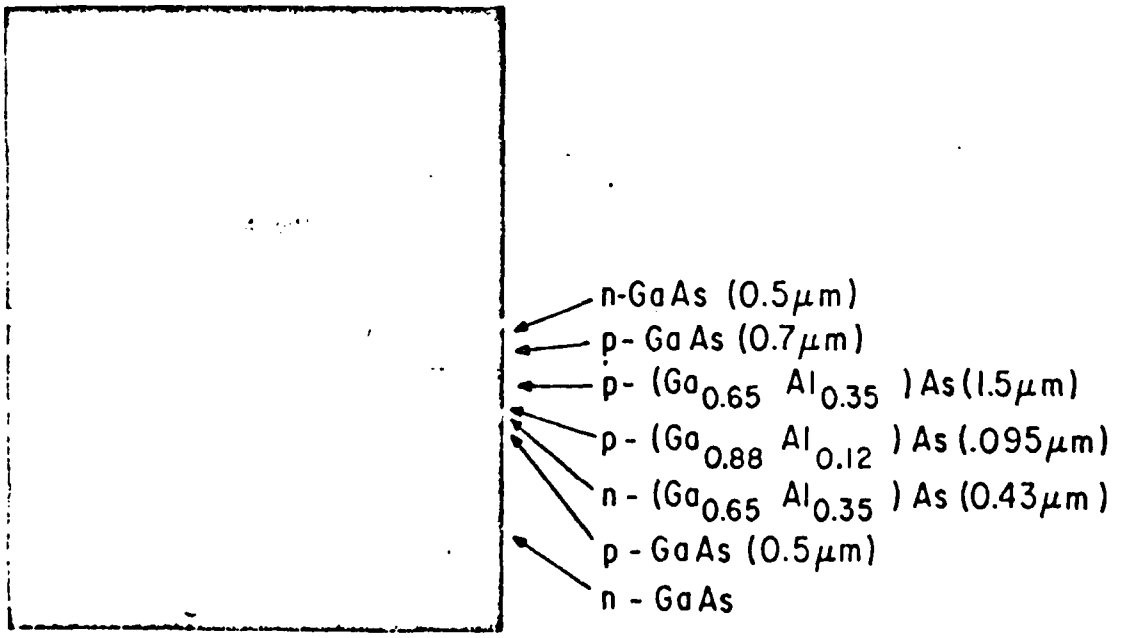
n-GaAs (0.5μm)
p-GaAs (0.7μm)
p-(Ga0.65 Al0.35)As (1.5μm)
p-(Ga0.88 Al0.12)As (.095μm)
n-(Ga0.65 Al0.35)As (0.43μm)
p-GaAs (0.5μm)
n-GaAs

(b)

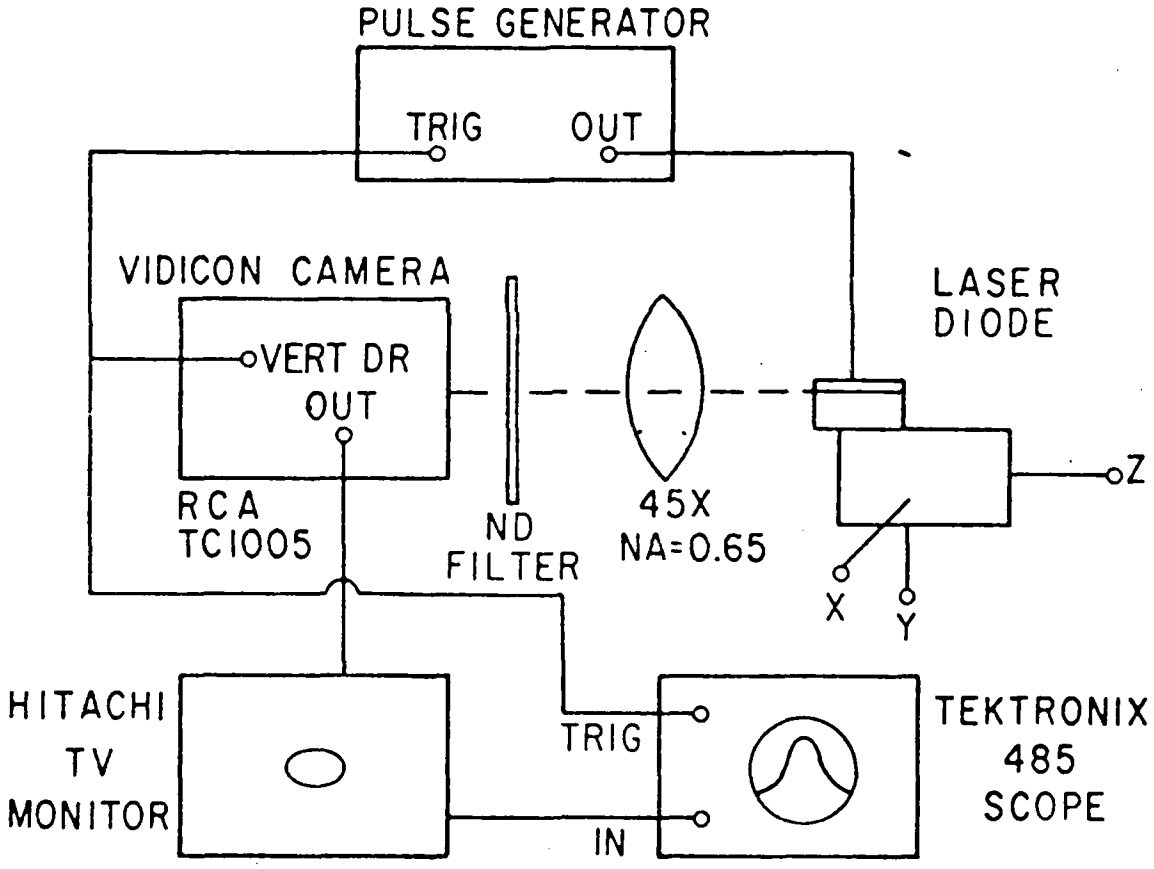
PULSE GENERATOR
TRIG
OUT
VIDICON CAMERA
VERT DR
OUT
RCA
TC1005
ND
FILTER
45X
NA=0.65
LASER
DIODE
Z
X
Y
HITACHI
TV
MONITOR
TRIG
IN
TEKTRONIX
485
SCOPE

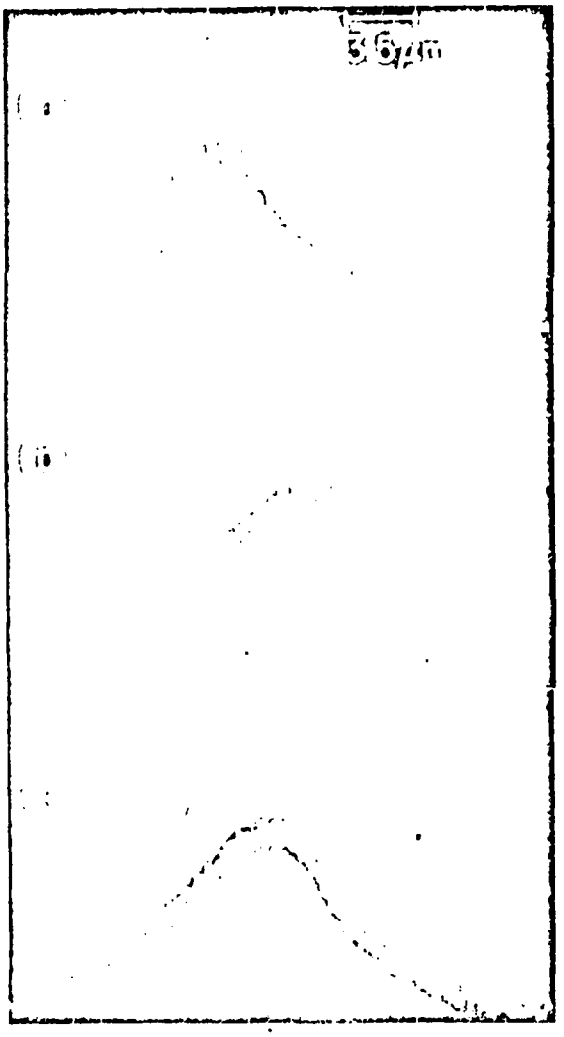

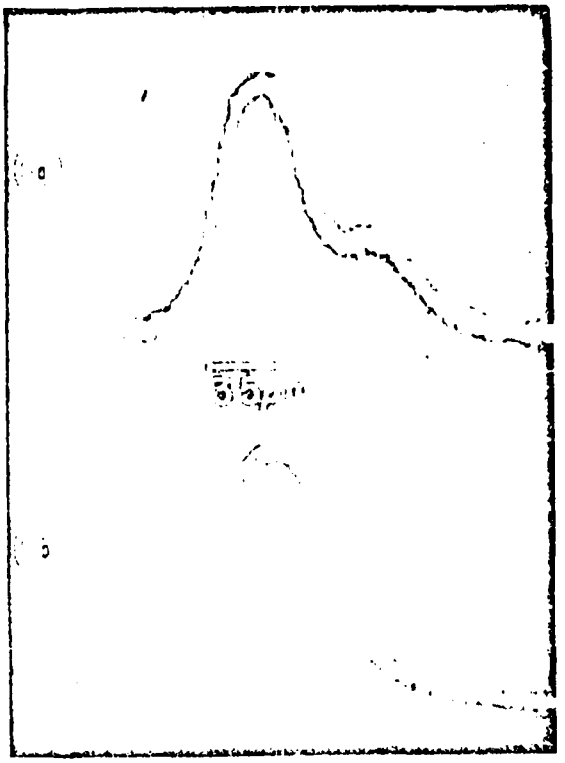

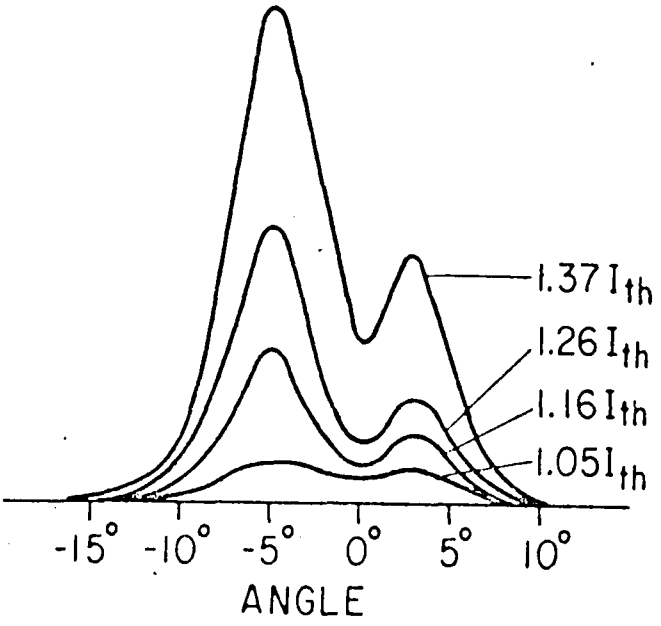
1.37 I_{th}
1.26 I_{th}
1.16 I_{th}
1.05 I_{th}
-15° -10° -5° 0° 5° 10°
ANGLE

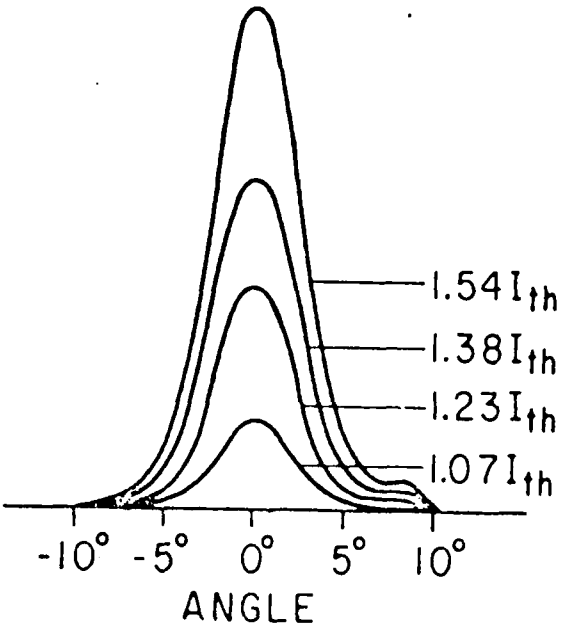
1.54 I_{th}
1.38 I_{th}
1.23 I_{th}
1.07 I_{th}
-10° -5° 0° 5° 10°
ANGLE

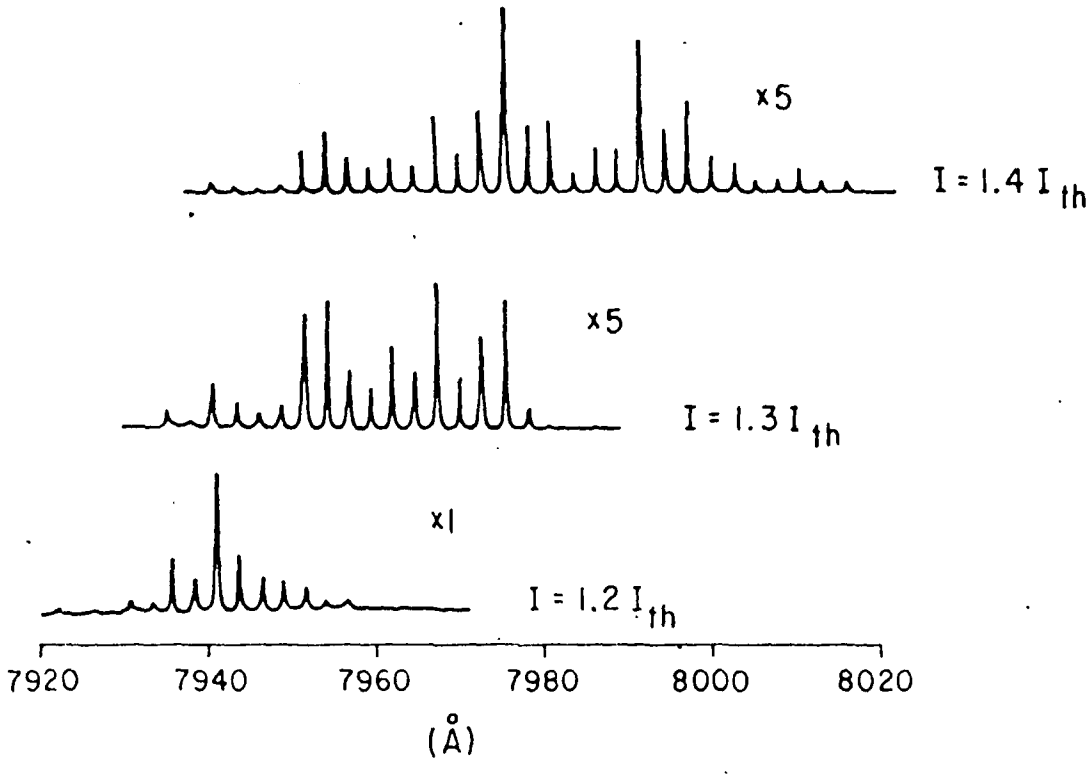
x5
I = 1.4 I th
x5
I = 1.3 I th
x1
I = 1.2 I th
7920
7940
7960
7980
8000
8020
(Å)

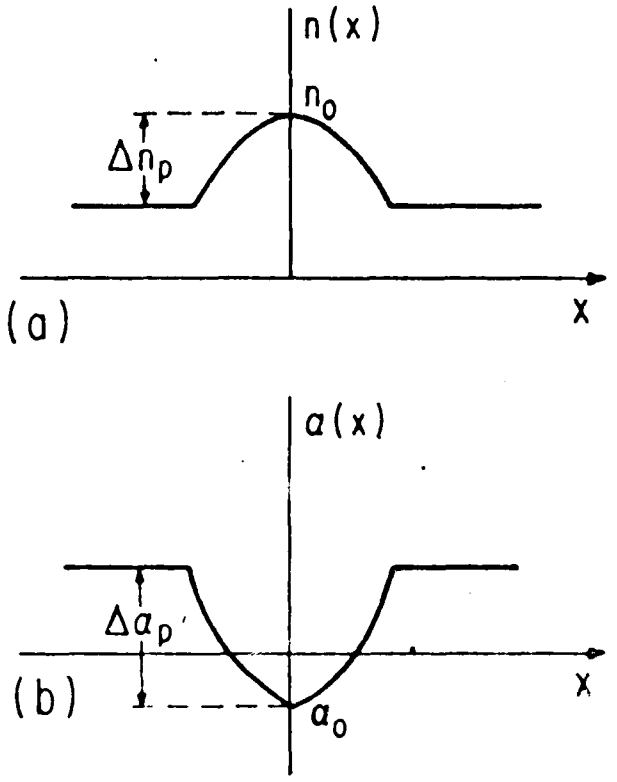
n(x)
n_0
Δn_p
(a)
x
α(x)
$\Delta \alpha_p$
(b)
x
α_0

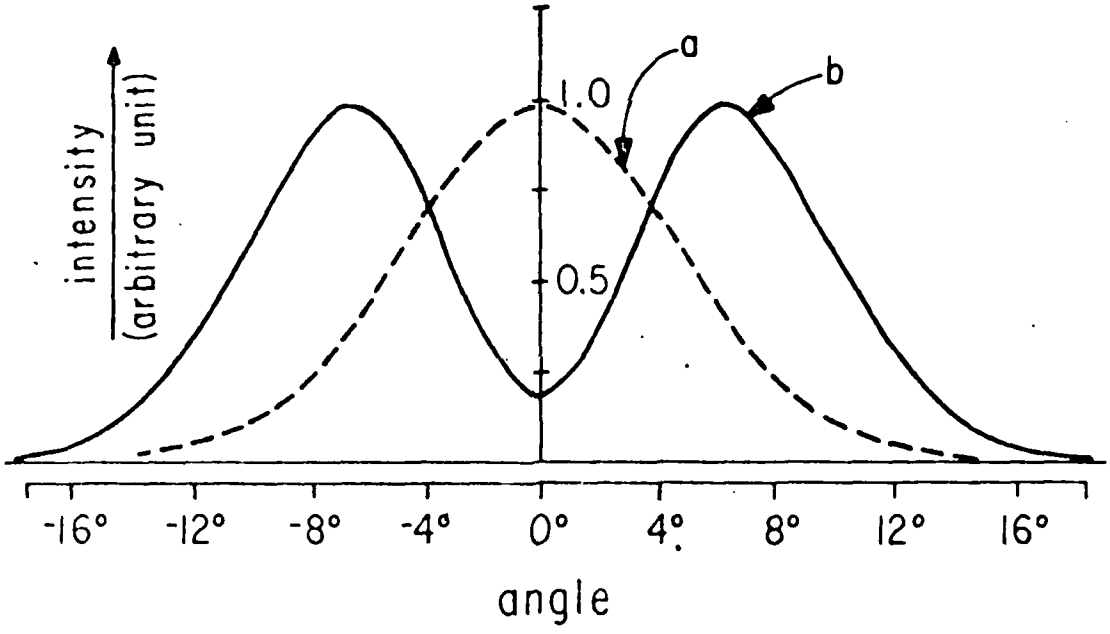
intensity
(arbitrary unit)
1.0
0.5
a
b
-16°
-12°
-8°
-4°
0°
4°
8°
12°
16°
angle

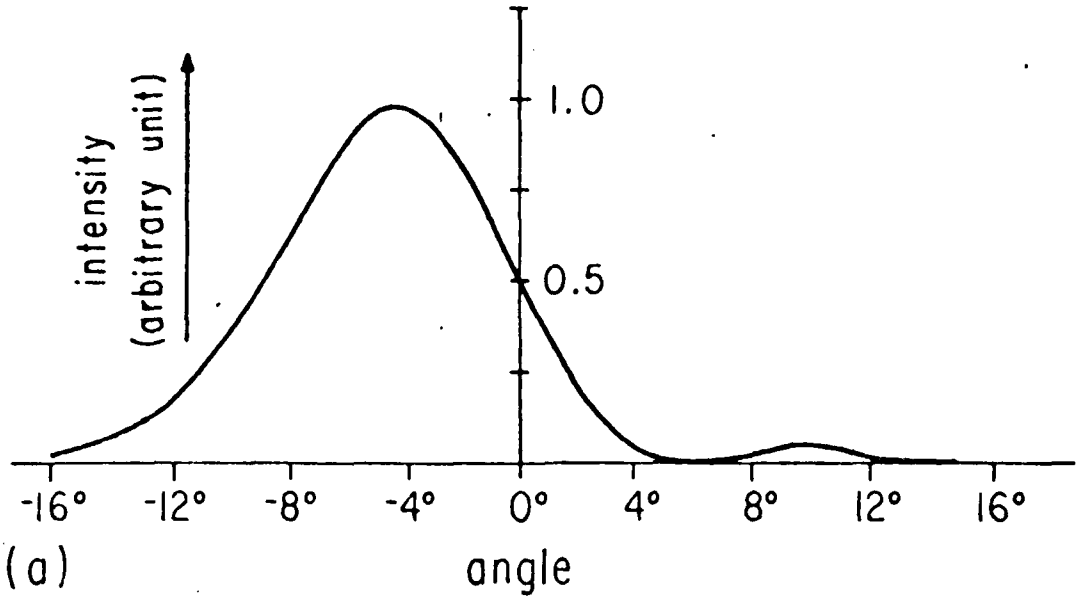
intensity
(arbitrary unit)
1.0
0.5
-16°
-12°
-8°
-4°
0°
4°
8°
12°
16°
angle

(a)

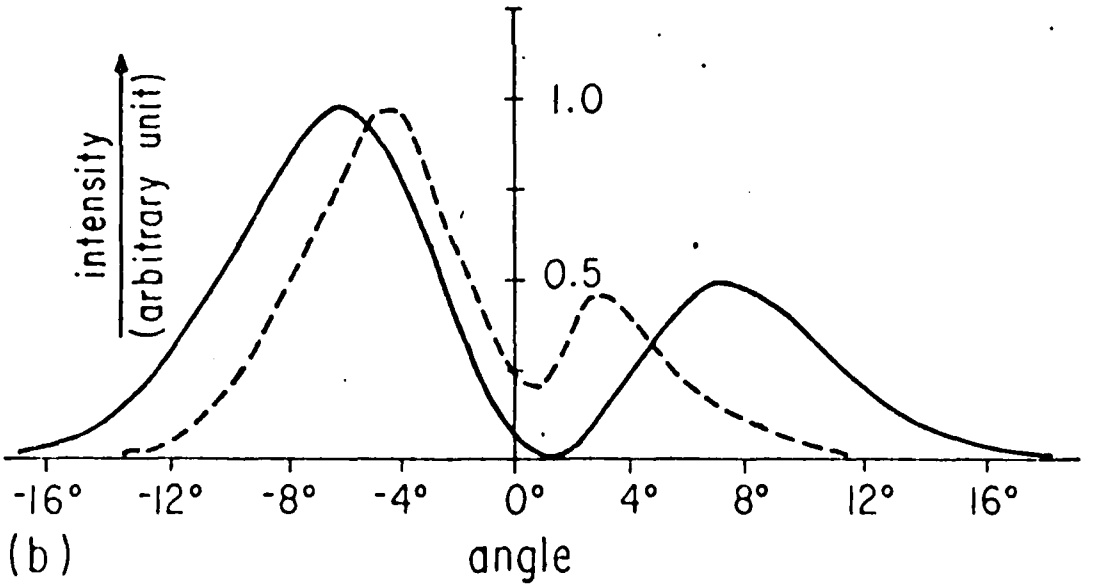
intensity
(arbitrary unit)
1.0
0.5
-16°
-12°
-8°
-4°
0°
4°
8°
12°
16°
angle

(b)


FILME